TIME FREQUENCY ANALYSIS – AN APPLICATION TO

FMCW RADARS

by

BALAJI NAGARAJAN

B.E., Electronics and Communication Engineering

Hindustan College of Engineering, University of Madras

Chennai, India – 2001

Submitted to the Department of Electrical Engineering and Computer

Science and the Faculty of the Graduate School of the University of Kansas

in partial fulfillment of the requirements for the degree of

Master of Science

Committee:

_____

Glenn Prescott: Chairperson

_____

Christopher Allen

_____

Swapan Chakrabarti

Date of Defense:27th Jan,2004

ABSTRACT

The Fourier transform of a signal defines the frequency domain representation of the signal in that it specifies relative amplitudes of the various frequency components of the signal. However, the Fourier transform is not always the best tool to analyze *'real-time signals'* which have frequency components that change over time. Joint time-frequency techniques were developed for characterizing the time-varying frequency content of the signal.

This project presents an overview of the basic concepts and well-tested algorithms for joint time-frequency analysis with particular reference to their application to radar signals. The time-frequency techniques can be classified into two types: linear (e.g., short-time Fourier transform, Gabor expansion, Wavelet transform) and quadratic (e.g., Wigner-Ville distribution, Cohen's class of distributions, Time-frequency distribution series). The aforementioned techniques are discussed in detail and are tested first against ideal simulations of normal cosine and chirp signals and then with the radar beat signal. A brief description of FMCW sea-ice radar developed in RSL, University of Kansas is given, and the data from this radar is used as experimental data to compare simulation results with measured sea-ice thickness levels. One of the important applications of time-frequency analysis is to exactly predict the occurrence of surface return layers and to distinguish it from noise signals and multiples. These techniques are also investigated for time-variant filtering of noise from the radar echogram and suitable recommendations are provided.

To my parents

&

brother

ACKNOWLEDGEMENTS

TABLE OF CONTENTS

LIST OF TABLES

LIST OF FIGURES

CHAPTER 1

1 INTRODUCTION

1.1 *What is Time-Frequency Analysis?*

The Fourier transform has become one of most widely used signal-analysis tools in real-time signal analysis. The fundamental idea behind the Fourier transform is that any arbitrary signal can be decomposed as a superposition of weighted sinusoidal functions. Its value at a particular frequency is a measure of the similarity of the signal to the sinusoidal basis at that frequency and hence the frequency attributes of the signal are exactly described. While the Fourier transform is a very useful concept for stationary signals, many signals encountered in real-world situations have frequency content that changes over time. One of the most common applications is speech & music signal processing, where the harmonic content of the acoustic signal changes for different notes. To represent signals of this nature, *Joint time-frequency transforms* were developed which characterized the exact behavior of the time-varying frequency content of the signal.

The most common time-frequency techniques such as Gabor expansion, wavelets [9] and time-dependant spectra have been developed and widely studied. In addition to being used for studying the time-dependant spectra, Joint Time-Frequency Analysis (JTFA) is also a very powerful tool for removing noise and interference from a signal.

In general, random noise tends to spread evenly in the joint time-frequency domain, while the signal itself concentrates in a relatively small range. Consequently, the signal-to-noise ratio (SNR) can be substantially improved in the joint-time frequency domain.

1.2 Applications of JTFA to Radar Signal Processing

Radar is an electromagnetic instrument used for the detection and location of targets, such as aircraft, ships and ground vehicles. Here, in our application, it is used to determine the thickness of sea-ice. It transmits electromagnetic energy to a target and processes the reflected signal from the target and clutter to produce a high-resolution image of the target. Any unwanted radar return that can interfere with the detection of the desired targets is referred to as clutter. To obtain a high-resolution radar image, a wide signal bandwidth and long imaging time are required. However, due to the time-varying behavior of the returned signal and due to the multiple scattering behavior of the target, the radar resolution can be significantly degraded and the image becomes blurred.

Conventional radar processing uses the Fourier transform to identify Doppler frequencies. In order to apply the Fourier transform, the Doppler frequency content of the radar data should be stationary over a given time interval. To satisfy these constraints and to obtain an exact image, complicated motion-compensation

algorithms are necessary to be implemented. Otherwise, the Fourier transform can cause the Doppler frequency spectrum to become smeared. Recently, Chen [2] introduced an approach using joint time-frequency transform to overcome the limitations caused by the Fourier transform. Replacing the conventional Fourier transform with a joint time-frequency transform, a high-resolution radar image can be achieved without applying complicated motion-compensation algorithms.

The development of high-resolution radar techniques has made it possible to generate a 1D down-range map of the target called the '*range profile*'. Similarly, by observing a target in relative motion with respect to the radar over a sufficient time interval, it is possible to generate a 1D cross-range map of the target. In simple targets, a range profile typically consists of a series of distinct peaks that can be related spatially to the isolated scattering centers on the target. These features are often utilized for target recognition features. In real targets, however, the scattering from some components on a target is not always well localized in time and may give rise to range-extended returns. The interpretation of these dispersive scattering phenomena is difficult to be handled in the time-domain range profile. Hence, joint time-frequency techniques are used for analyzing these range profiles by exactly characterizing the top & bottom of the range profiles over all instances of time at a given frequency.

1.3 FMCW radars to measure sea ice thickness

Sea ice thickness measurements play an important role in monitoring global climate change. Recently, there has been a considerable thinning of the artic sea ice as indicated by studies using submarine sonar profiling. But, these measurements suffer from limited temporal and spatial coverage. Air borne measurements using Very High Frequency (VHF) pulse radars did not have sufficient range resolution to resolve the ice-water interface and air-ice interface for ice with a thickness of less than 2m i.e. the earlier radars used were not optimized for the application.

The Radar Systems and Remote Sensing Laboratory (RSL) at the University of Kansas have been successful in designing and developing a Frequency Modulated Continuous Wave (FMCW) radar system that can achieve the required resolution. The electromagnetic simulations suggested operating an FMCW radar over 50-250 MHz for measuring thick first-year or multiyear sea-ice thickness in the Arctic region and 300-1300 MHz for measurements in the Antarctic region and thin sea ice in the Arctic. The system was successfully tested through numerous field trials.

1.4 Organization of Project

This report has been organized into five chapters. Chapter 1 outlines the entire project giving an introduction to the need for time-frequency analysis and its application to radar signal processing. Chapter 2 provides the radar system background, describing the FMCW radar and how it is used. Also in this chapter, the drawbacks of the

Fourier spectral analysis that necessitates the need for using JTFA techniques is discussed. Chapter 3 describes the time-frequency techniques used in this project, and explains their advantages and disadvantages. There is also a brief introduction to time-variant filtering techniques. Chapter 4 presents and explains the results of signal processing experiments conducted on sea-ice radar data based on several time-frequency techniques and Chapter 5 summarizes the project and provides suggestions for future recommendations & improvement.

CHAPTER 2

2   BACKGROUND

2.1   Radar System Design

A prototype radar system operating in the Frequency-Modulated Continuous Wave (FM-CW) mode was designed to operate in the two frequency ranges mentioned above. Here, for our analysis, we consider the radar operating in the frequency range 50-250 MHz. The system designed was a modified version of a 50-2000 MHz FMCW radar developed at RSL to map near-surface internal layers over the Greenland ice sheet to estimate the accumulation rate [11]. Figure 1 shows the functional block diagram of the radar system.

The salient features of the radar include: a transmitter, which generates a linearly chirped signal of frequency 4.5-6 GHz (wideband).The signal was down-converted to the desired frequency range of 50-250 MHz after mixing with the signal from the receiver. At the receiver, low-gain & high-isolation amplifiers were used to provide the required gain, antennas with minimum ringing and low return loss improved the system performance and sensitivity.
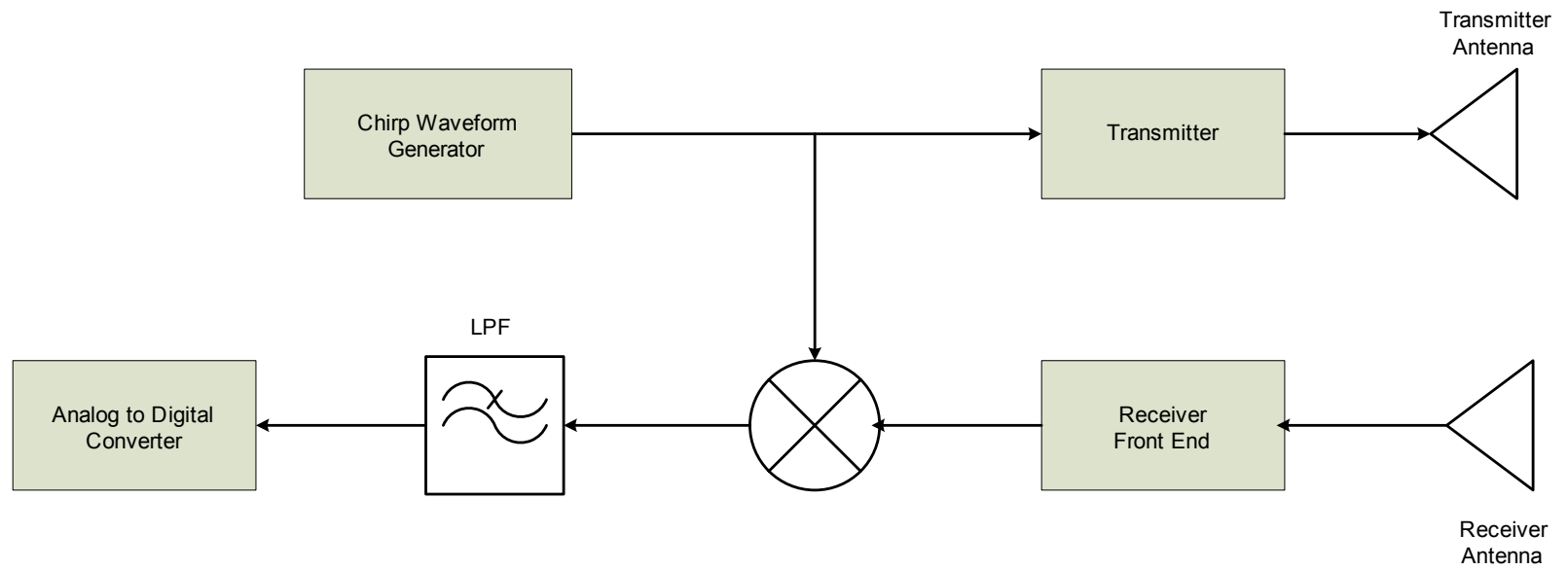
Figure 1: Functional Block Diagram of Sea-ice Radar System

2.2 Radar System Specifications

The radar system was calibrated to operate in the VHF frequency range (50-250 MHz). The prototype system was mounted on a sled that was built at RSL and collected data over sea-ice located off Barrow, Alaska. Some of the important radar parameters are listed below in Table1.

System Parameters	Value
Modulation	Swept FM
Chirp Frequency Range	50-250 MHz,
Unambiguous Range	3-30 meters
Transmit Power	20 dBm
Chirp Time	5 ms
Range Resolution	75 cm

Table 1: System specifications of the sea-ice radar

A Compact Low-Power Radar Data Acquisition system (DAC) [12] was used for this FMCW sea-ice radar that is capable of automating the data acquisition process, controlling the radar and processing the data. The digital system is composed of a signal generator and data acquisition system. The digital system has a high-resolution 16-bit analog-to-digital converter that can sample the beat frequencies at a maximum clock frequency of 5 MHz.

2.3 Calculation of Beat Frequency
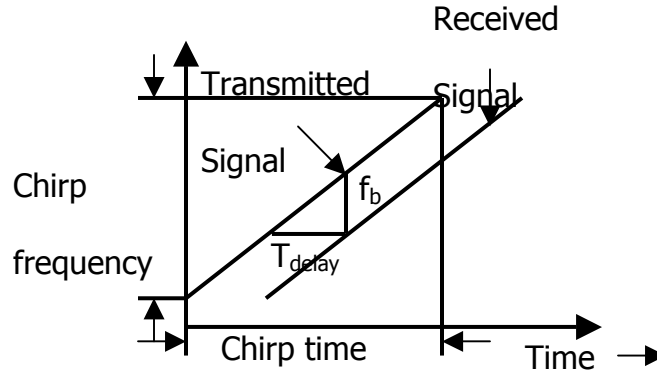
Figure 2: FMCW operation of Radar system

A common way of increasing the pulse energy while still maintaining the high resolution of radar is to apply a *chirp* waveform which is a sine wave with linearly increasing/decreasing frequency. If the linear FM waveform is made much longer than 2-way propagation delay, it is often termed *frequency-modulated continuous wave*. Hence, the frequency, $f(t)$ of a chirp is given by

$$f(t) = f_0 + \alpha t \tag{1}$$

where f_0 is the start frequency and α is the chirp rate [Hz/s]. In this case, the receiver has to start receiving the backscattered signals while the transmitter is still transmitting. The received echoes are homodyned (mixed) with a replica of the transmitted waveform to produce a beat signal as shown in Figure 2. When more than one target is present within the view of the radar, the mixer output will contain more than one difference frequency. Since the system is linear, there will be a frequency component corresponding to each target. In

9

principle, the range to each target may be determined by measuring the individual frequency components. The beat frequency f_b becomes proportional to the target delay T_{DELAY}.

$$\frac{f_b}{BW} = \frac{T_{DELAY}}{t_{CHIRP}}$$
$$\alpha = BW / t_{CHIRP}, T_{DELAY} = 2R / c \qquad \textbf{(2)}$$
$$\Rightarrow f_b = \frac{2R \times BW}{c \times t_{CHIRP}}$$

The I & Q output of the homodying quadrature mixer is narrowband compared to the radar waveform, and typically low speed A/D-converters operating with sampling frequencies in the kHz range can be used for data acquisition.

2.4 Need for Time-Frequency Analysis of Radar Range Profiles

The Fourier spectrum of a radar range profile illustrates the variation of signal amplitude in decibels over the distance traveled by the radar signal. Figure 3 shows the Fourier spectrum of a particular Amplitude scope (A-scope) display of the sea-ice radar profile.
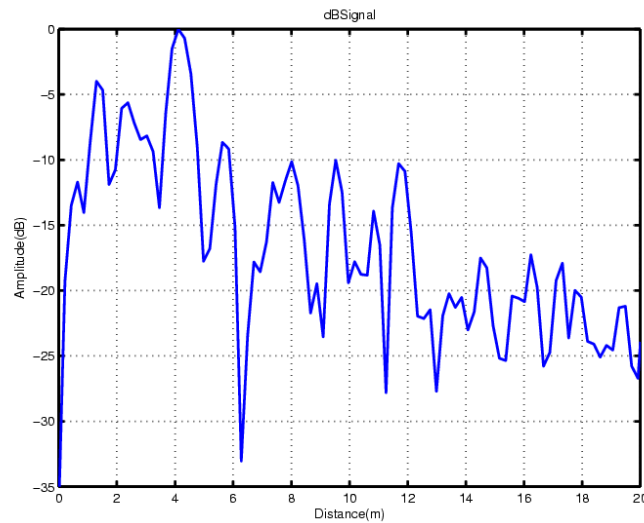
Figure 3: A-scope of particular range profile

10

We can see clearly signals of varying amplitude in the spectrum with the highest signal amplitude at 0dB indicating the antenna feed through or *Top* of the range profile. The location of this surface return at the specified distance is based on calculations given in Equation (2) and from data recorded in field tests. The problem with the Fourier spectrum is that we are not able to exactly predict the occurrence of the ice-bottom and distinguish it from the noise and multiple returns that might be occurring along with the desired signals. This is because the noise and multiple returns might be larger in amplitude compared to the *ice-bottom* leading to improper determination of the depth from the radar compared to the measured field data. The time-frequency spectrum gives a two dimensional analysis of the exact position of the layers of the range profiles. This indicates the position of different layers at a particular frequency along with the position in time simultaneously. The time-frequency transform makes it easier to distinguish between the *top* and *bottom* of the range profiles from their corresponding multiples and noise returns. These transforms can also be used for time-varying filtering procedures for separating the noise from the data signal.

We will be explaining in detail about different time-frequency techniques used for signal processing experiments in *Chapter 3* with their respective advantages and disadvantages. *Chapter 4* deals with testing these techniques, initially with ideal simulations and then with experimental radar data compare the results observed with those that were measured when field tests were conducted.

CHAPTER 3

3   TIME-FREQUENCY REPRESENTATION (TFR)

3.1 Introduction

Time-Frequency methods are powerful tools for radar signal processing because most radars are used for determining the range to a target, which is a function of time, and the target speed which is a function of frequency. The Radar has two time scales, fast time scale and slow time scale [4]. These correspond to the signal transmission into the medium and the movement of the radar respectively. The radar signal is transmitted once every Pulse Repetition Interval (PRI). Within each PRI, the signal travels through the medium and this time is termed as *fast time*. The radar's next transmission occurs from a different azimuthal position as the radar is moving albeit at a very slow rate compared to the speed of the signal. This corresponds to the *slow time*.

In this chapter, we provide an overview of various time-frequency transforms developed in the signal processing community. Time-frequency techniques are broadly classified into two categories: Linear transforms & Quadratic (or bilinear) transforms. A flowchart showing the basic classification is given below in Figure 4. In Section 3.2, we first discuss linear time-frequency transforms. The discussion commences with the Short-Time Fourier Transform (STFT), Gabor expansion in detail and moves onto two other linear transforms, the adaptive

time-frequency representation and a brief summary about the continuous wavelet transform. Linear transforms are mainly characterized by the STFT and wavelet transforms. The linear transformations are realized by comparing the analyzed signal with a set of selected elementary functions viz. frequency modulation in the STFT and by scaling the center frequency of the mother wavelet in the wavelet transform. The inverse of sampled STFT can be accomplished by the Gabor expansion.

```
                    ┌─────────────────┐
                    │  Time-Frequency │
                    │    Techniques   │
                    └─────────────────┘
                      /            \
          ┌──────────────────┐   ┌──────────────────┐
          │ Linear Transforms│   │     Quadratic    │
          │                  │   │    Transforms    │
          └──────────────────┘   └──────────────────┘
           /      |      \         /       |        \
```

| Short-time Fourier Transform (STFT) | Gabor Expansion | Continuous Wavelet Transform (CWT) | Wigner-Ville Distribution (WVD) | Cohen's Class of Distributions | Time-Frequency Distribution Series (TFDS) |
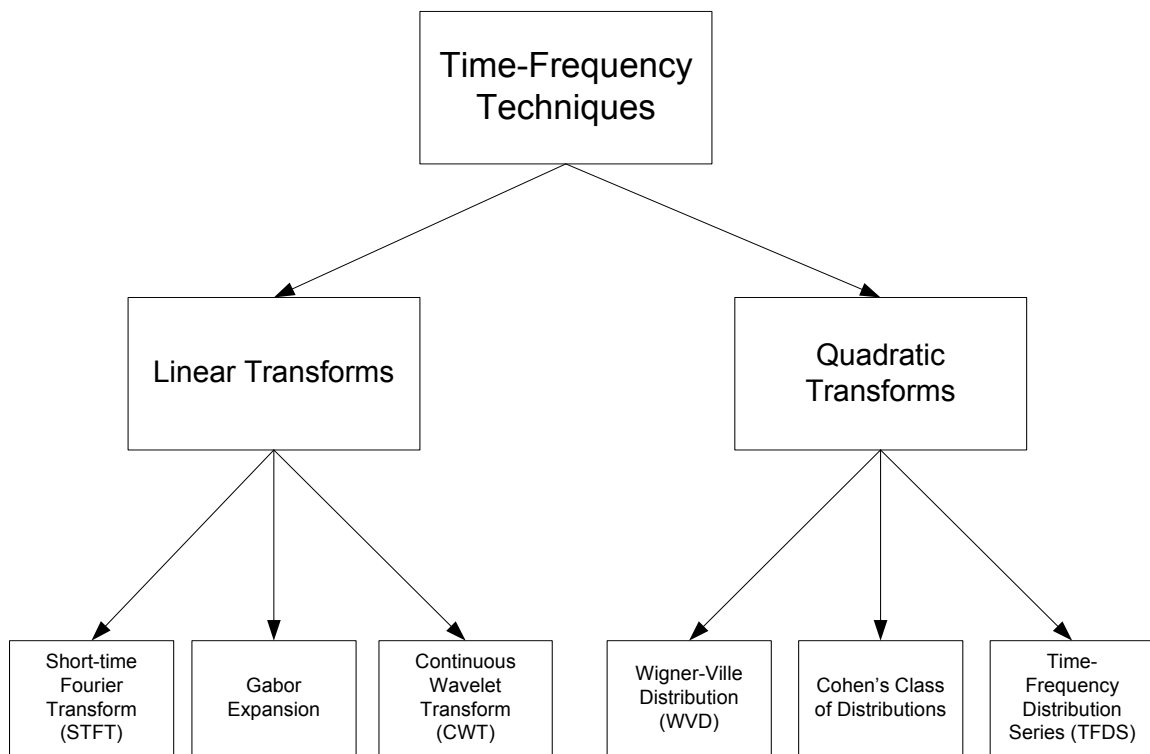
Figure 4: Classification of the different time-frequency techniques

In Section 3.3, we discuss quadratic time-frequency transforms. We begin with the Wigner-Ville distribution and discuss Cohen's class of distributions. The bilinear time-frequency representations are characterized by a number of distributions, the most common one being

the Wigner-Ville distribution (WVD) because of its simplicity and better characterization of the signal's time-dependant spectra than the STFT spectrogram (which is squared magnitude of the short-time Fourier transform) and scalogram (which is square of the wavelets). The problem of the WVD is the cross-term interference that significantly hinders its applications in signal analysis. On the other hand, the useful properties of the WVD are all obtained by averaging the Wigner-Ville distribution. These observations suggest that if the WVD is thought as the sum of localized 2D (time and frequency) harmonic functions, then its useful properties will mainly depend on the low oscillated harmonics. This is because low harmonics have larger averages. The high harmonics directly relate to the cross-term interference and are less important to the joint time-frequency representations. Hence, we may apply a lowpass filter for the WVD, to retain the low frequency components and remove the high frequency parts. Since the high frequency parts have small averages, the lowpass filtered Wigner-Ville distribution has reduced cross-term interference. There are two types of lowpass filters: linear, characterized by Cohen's class and non-linear characterized by the time-frequency distribution series.

Another main advantage in analyzing radar signals in the time-frequency domain is for noise reduction. A time-variant filtering technique can be employed which significantly improves the signal-to-noise ratio and produces a noise-reduced TFR. This has been particularly useful for wideband and non-stationary signal estimation. Both linear and bi-linear transformations could be used as time-variant filters but the Gabor expansion is most powerful and simple tool. The aforementioned techniques will be discussed in detail with their applications in the

14

forthcoming sections and a comparative analysis will be provided. The time-variant techniques and their usefulness will also be described with their limitations and suggested alternatives.

3.2 Linear Time-Frequency Transforms

Linear time-frequency transforms can be understood by first reviewing the Fourier transform. The Fourier transform of a signal *s(t)* is defined as

$$S(\omega) = \int_{-\infty}^{+\infty} s(t) \exp\{-j\omega t\} dt \tag{3}$$

where $\omega = 2\pi f$ is the angular frequency. $S(\omega)$ can be interpreted as the projection of the signal onto a complex exponential function $\exp\{-j\omega t\}$ at angular frequency ω. Since the set of exponentials form an orthogonal basis set, the original function can be constructed from the projection values by the process of

$$s(t) = \frac{1}{2\pi} \int_{-\infty}^{+\infty} S(\omega) \exp\{j\omega t\} d\omega \tag{4}$$

which is the inverse Fourier transform of $S(\omega)$. When we use (3) to estimate the frequency spectrum of a signal, we assume that the frequency content of the signal is relatively stable during the observation time interval. If the frequency content changes with time, it is not possible for the frequency spectrum to uniquely represent and characterize the signal. In the following subsections, three linear time-frequency transforms (viz. STFT, Gabor Expansion, and CWT) are presented. They can be considered as a generalization of the Fourier transform

with alternative basis sets that can better reflect the time-varying nature of the signal frequency spectrum.

3.2.1 Short-time Fourier transform (STFT)

The basis functions used in Fourier analysis do not explicitly reflect a signal's time varying nature. Hence, the STFT was developed which modified the Fourier transform by comparing the signals with elementary functions that are localized in time and frequency domains simultaneously, i.e.

$$STFT(t,\omega) = \int s(\tau)\gamma_{t,\omega}^{*}(\tau)d\tau = \int s(\tau)\gamma^{*}(\tau - t)e^{-j\omega\tau}d\tau \qquad (5)$$

which is a regular inner product and reflects the similarity between signal *s(t)* and the elementary function $\gamma(\tau - t)\exp\{-j\omega\tau\}$. The function $\gamma(t)$ usually has short time duration and thereby it is named as the *window function.* Equation (5) is called *short-time Fourier transform* (STFT) or windowed Fourier transform.
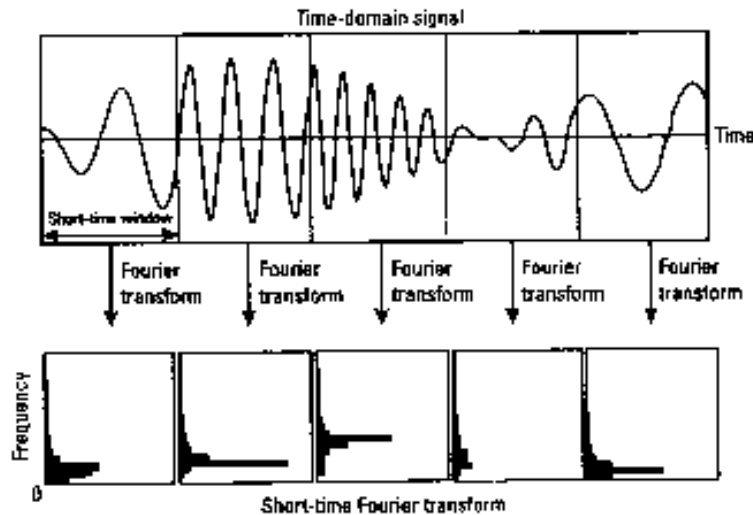
Figure 5: Illustration of STFT (Courtesy: Time-frequency Transforms by Chen-Ling)

16

Figure 5 depicts the procedure of computing the STFT. Instead of processing the entire signal in a single frame, the STFT takes the Fourier transform on a block-by-block basis. Therefore, the resulting Fourier transform can be described as a signal's frequency behavior during the time period covered by the data block. It can be seen as first multiplying the function $\gamma(t)$ with signal $s(t)$ and computing the Fourier transform of the product $s(\tau)\gamma^*(\tau - t)$. Because the window function $\gamma(t)$ has short time duration, the Fourier transform of $s(\tau)\gamma^*(\tau - t)$ reflects the signal's local frequency properties. By moving $\gamma(t)$ and repeating the same process, we could obtain an idea how the signal's frequency contents evolve over time. The analysis window function $\gamma(t)$ balances the time and frequency resolutions. The smaller the time duration of $\gamma(t)$, the better the time resolution (poorer frequency resolution) and vice-versa. The blocks could be overlapped or disjointed. The percentage of overlap between each block is determined by the time sampling step *T* and the length of the analysis window function $\gamma(t)$. The effects of the window function on real-time data are shown in *Chapter 4*, measurement results are compared against theoretical analysis and supporting conclusions are provided.

The squared magnitude of the STFT is known as the *STFT spectrogram*. The STFT spectrogram is the most simple and often used time-dependent spectrum, which depicts a signal's energy distribution in the joint time-frequency domain. While the STFT in general is complex, the spectrogram is always real-valued.

Given $STFT(t,\omega)$ for all t and ω, we can completely recover the signal $s(t)$ as

$$s(t) = \frac{1}{2\pi\gamma(0)} \int STFT(t,\omega) \exp\{j\omega t\} d\omega \qquad (6)$$

The signal can also be reconstructed from the sampled version of the short-time Fourier transform, $STFT(mT, n\Omega)$ where T and Ω denote the time and frequency sampling steps, respectively. This can be represented as

$$STFT(mT, n\Omega) = \int_{-\infty}^{+\infty} s(t)\gamma^*(t - mT)e^{-jn\Omega t} dt \qquad (7)$$

which is quite similar to equation (5). This equation is particularly useful in determining the relationship between STFT and the Gabor expansion, which is explained in detail in the next section.

3.2.2 Gabor Expansion

Dennis Gabor, a British physicist suggested expanding a signal into a set of functions that are concentrated in both the time and frequency domains and then use the coefficients as the description of the signal's local property [3]. For signal $s(t)$, the Gabor expansion is defined as

$$s(t) = \sum_{m=-\infty}^{\infty} \sum_{n=-\infty}^{\infty} C_{m,n} h_{m,n}(t) \qquad (8)$$

where $C_{m,n}$ are called the Gabor coefficients.

18

The set of elementary functions $h_{m,n}(t)$ consists of a time- and frequency-shifted function $h(t)$, i.e.

$$h_{m,n}(t) = h(t - mT)e^{jn\Omega t} \tag{9}$$

A function's time and frequency properties are not independent i.e. we can't find a function that has arbitrarily short time duration and narrow frequency bandwidth at the same time. Similarly, if a function has short time duration, its frequency bandwidth must be wide, or vice versa. From the uncertainty principle point of view, it is the Gaussian type signal such as

$$g(t) = \left(\frac{\alpha}{\pi}\right)^{\frac{1}{4}} \exp\left\{-\frac{\alpha}{2}t^2\right\} \tag{10}$$

that achieves the optimal joint time-frequency concentration. The balance of the time and frequency concentration is controlled by the parameter α. The smaller the value of α, the narrower the frequency bandwidth (longer time duration) and vice-versa. Hence, Gabor selected the Gaussian-type signal $g(t)$ as the elementary function .The product of TΩ determines the density of the sampling grid. The smaller the product, the denser the sampling. The necessary condition for the existence of the Gabor expansion is that the sampling cell TΩ must be small enough to satisfy

$$T\Omega \leq 2\pi \tag{11}$$

When the product $T\Omega = 2\pi$, it is considered *critical sampling* and gives the most compact representation. When $T\Omega < 2\pi$, it is considered to be oversampling.

The continuous-time inverse STFT is a highly redundant expansion. In applications, for a compact representation, we usually use sampled STFT. However, the imprudent choice of analysis function $\gamma(t)$ and sampling steps, T and Ω, may lead to the sampled STFT being non-invertible. With the help of the Gabor expansion, we overcome the problem of inverse of sampled STFT. To characterize the signal's behavior in the time and frequency domains simultaneously, the elementary functions need to be localized in both time and frequency domains and if the set of elementary Gabor functions $\{h_{m,n}(t)\}$ is complete, then there will be a dual function $\gamma(t)$ such that we can rewrite equation (7) in the inner product form to compute the Gabor coefficients as

$$C_{m,n} = \int s(t)\gamma_{m,n}^{*}(t)dt = \int s(t)\gamma^{*}(t-mT)\exp\{-jn\Omega t\}dt$$

$$= STFT(mT, n\Omega)$$

$$(12)$$

Equations (8) and (12) form a pair of Gabor expansions and indicate that the STFT is, in fact, the Gabor coefficient. Conversely, the Gabor expansion can be thought of as the inverse of the STFT. Thus, for a given time function $s(t)$ and analysis window function $\gamma(t)$, we are always able to find the joint time-frequency function $C_{m,n}$. At critical sampling, the set of $\{h_{m,n}(t)\}$ is linearly independent and we say that $\gamma(t)$ and $h(t)$ are biorthogonal to each other. For oversampling, the set of $\{h_{m,n}(t)\}$ is linearly dependant. It becomes difficult to compute the dual function $\gamma(t)$ for a given $h(t)$. This led to the development of the *Discrete Gabor Expansion*, which will be explained in detail below.

3.2.2.1 Discrete Gabor Expansion

The Gabor Expansion for discrete samples is derived by applying the sampling theorem and Poisson-sum formula as

$$s[i] = \sum_{m} \sum_{n=0}^{N-1} C_{m,n} h[i - m\Delta M] W_N^{ni} \tag{13}$$

where

$$W_N^{ni} = \exp\left\{ j\frac{2\pi ni}{N} \right\} \text{ and } C_{m,n} = \sum_{i} s[i]\gamma^*[i - m\Delta M] W_N^{-ni} \tag{14}$$

where ΔM denotes the discrete time sampling interval. N indicates the number of frequency channels. The ratio $N/\Delta M$ is considered as the oversampling rate. For a stable reconstruction, the oversampling rate must be more than or equal to one. Usually, we require that L is evenly divisible by N and ΔM. The number of frequency bins N is a power of two. When the signal length is equal to the length of $h[i]$ and $\gamma[i]$, the solution of $\gamma[i]$ almost always exists!

3.2.2.2 Orthogonal-Like Gabor Expansion

For the case of critical sampling $(N = \Delta M)$, the solution of $\gamma[i]$ and hence $C_{m,n}$ is unique. The Gabor coefficients $C_{m,n}$ are the sampled short-time Fourier transform with the window function $\gamma[i]$. This means that the window function has to be localized in the joint time-frequency domain. Otherwise, the Gabor coefficients $C_{m,n}$, inner product of $s[i]$ & $\gamma[i]$, would not characterize the signal's local behavior. Because the Gabor elementary function

h[i] tends to be optimally concentrated, an optimal value for the analysis window function is chosen which minimizes the least square error as given by the relation

$$\min_{dualrelation} \left\| \frac{\bar{\gamma}}{\left|\bar{\gamma}\right|} - \bar{h} \right\|^2$$

(15)

The difference between *h[i]* and $\gamma_{opt}[i]$ is inversely proportional to the sampling rate. As the oversampling rate increases, $\gamma_{opt}[i]$ becomes closer to *h[i]*. In this case, the Gabor coefficients $C_{m,n}$ are indeed the orthogonal projection on $\{h_{m,n}[i]\}$. For the orthogonal-like Gabor expansion, the Gabor coefficients $C_{m,n}$ will well characterize the signal's behavior in the vicinity of $[m\Delta M, n]$ as long as $h_{m,n}[i]$ is concentrated in $[m\Delta M, n]$.

Thus, we find that although Gabor did not investigate the inverse of the STFT, the Gabor expansion turns out to the most elegant algorithm of computing the inverse of a sampled STFT. The discrete Gabor expansion can be easily implemented with the help of elementary linear algebra. The orthogonal-type expansion is not only fundamental for time-frequency analysis but is particularly useful in *time-variant filtering* which will be discussed in later sections.

3.2.3 The Continuous Wavelet Transform (CWT)

The continuous wavelet transform was developed as an alternative approach to the short-time Fourier transform because the spectrogram is limited in resolution by the extent of the sliding window function. The wavelet analysis is done in a similar way to the STFT analysis, the signal is multiplied with a function (i.e. the wavelet), similar to the window function in the STFT, and the transform is computed separately for different segments of the time-domain signal. However, there are two main differences between the STFT and the CWT:

1. The Fourier transforms of the windowed signals are not taken, and therefore single peak will be seen corresponding to a sinusoid, i.e., negative frequencies are not computed.

2. The width of the window is changed as the transform is computed for every single spectral component, which is the most significant characteristic of the wavelet transform.

The continuous wavelet transform is defined as follows

$$CWT_x^{\psi}(\tau,s) = \Psi_x^{\psi}(\tau,s) = \frac{1}{\sqrt{|s|}} \int x(t)\psi^* \left(\frac{t - \tau}{s} \right) dt \qquad \textbf{(16)}$$

where $\psi(t)$ denotes the *mother wavelet*. The parameter *s* represents the scale index that is the reciprocal of frequency and the parameter τ indicates the time shifting (or translation). High scales (low frequencies) correspond to the global information of a signal that usually spans the entire signal, whereas low scales (high frequencies) correspond to detailed information of a hidden pattern in the signal that usually lasts for a relatively shorter time. In the two

dimensional case, the filtering is applied along each axis separately, thereby isolating the high and low frequency data in both dimensions. By using multiple scales, both the small-scale and large-scale details can be clearly represented and located, localizing the signal aspects in both time (or space, in this case) and frequency. An oft-used analogy is that the *'wavelet transform enables a person to see both the forest (the large scale) and the trees (the small scale)'.*

3.2.3.1 Wavelet Denoising

The wavelet transform has come to prominence in recent years because of its flexibility and usefulness in a wide variety of applications, such as compression, signal analysis, and the primary being *wavelet denoising*. In denoising, the wavelet coefficients at each scale are analyzed and altered to remove noise and, in some cases, enhance the signal. The theoretical basis for this wavelet denoising is the principle of noise decorrelation wherein the energy in a given signal is compressed into a few coefficients in the wavelet domain while the white noise remains equally distributed throughout the coefficients. The coefficients are then thresholded, that is, the coefficients with amplitudes below a certain threshold are set to zero, while the larger coefficients are either uniformly reduced, as in soft thresholding, or are left the same, as in hard thresholding. The inverse wavelet transform is then applied to return the signal to the original domain.

One way of understanding the seemingly contradictory goals of denoising without image blurring is that high-frequency, low-amplitude data in a signal is usually noise, or at least can

be removed without affecting the information conveyed by signal or image noticeably, but high-frequency, high-amplitude data usually is an important part of the signal, such as the edge of an object. Low-frequency data, at whatever intensity, does not usually contain noise, so the highest scale data, representing general trends in the signal, is typically not thresholded. The comparison of wavelet denoising and the time-variant filtering techniques are presented in *Chapter 4* and the results are summarized for radar data.

3.3 Bilinear Time-Frequency Transforms

The signal's energy distribution in the joint time-frequency domain is represented by the *time-dependant power spectrum*. It is given by the Fourier transform of the time-dependant auto-correlation function $R(t,\tau)$, with respect to variable τ i.e.

$$P(t,\omega) = \int R(t,\tau)\exp\{-j\omega\tau\}d\tau \qquad\qquad \textbf{(17)}$$

The most popular time-dependant power spectrum is the *STFT spectrogram*, which is the square of the short-time Fourier transform. The main problem of this spectrogram is that it suffers from the window effect wherein the width of $\gamma(t)$ governs the resulting time and frequency resolutions. This concept is discussed with illustrations for radar beat signals in *Chapter 4*.The distributions derived from the power spectrum are termed as quadratic (or bilinear) time-frequency distributions. In this section, we shall discuss two such time-frequency transforms, the WVD and Cohen's class of distributions.

3.3.1 The Wigner-Ville Distribution (WVD)

The WVD was originally developed in the area of quantum mechanics and then introduced for signal analysis by a French Scientist Ville. In the WVD, the time-dependant auto-correlation is given by

$$R(t,\tau) = s\left(t + \frac{\tau}{2}\right)s^*\left(t - \frac{\tau}{2}\right) \tag{18}$$

Substituting the above time-dependant auto-correlation into (17) yields

$$WVD_s(t,\omega) = \int s\left(t + \frac{\tau}{2}\right)s^*\left(t - \frac{\tau}{2}\right)\exp\{-j\omega\tau\}d\tau \tag{19}$$

Equation (19) is usually called the auto-WVD. Accordingly, the cross-WVD is defined as

$$WVD_{s,g}(t,\omega) = \int s\left(t + \frac{\tau}{2}\right)g^*\left(t - \frac{\tau}{2}\right)\exp\{-j\omega\tau\}d\tau \tag{20}$$

where *s(t)* and *g(t)* denote two different signals.

The important properties of the WVD are:

1. The WVD of any signal is always real.

2. Satisfies the time marginal & frequency marginal condition i.e. by summing the time-frequency distributions over all frequencies, we obtain the instantaneous energy of the signal at a particular instance and by summing the time-frequency distributions over all time, we obtain the power spectrum of the signal at a particular frequency.

3. The mean frequency computed from the WVD is equal to the derivative of the phase i.e. the signal's average instantaneous frequency

4. Energy of the WVD is the same as the energy content in the signal i.e.,

$$\frac{1}{2\pi} \int\limits_{-\infty}^{\infty} \int\limits_{-\infty}^{\infty} WVD(t,\omega)dtd\omega = \int\limits_{-\infty}^{\infty} |s(t)|^2 dt = \frac{1}{2\pi} \int\limits_{-\infty}^{\infty} |S(\omega)|^2 d\omega \qquad \textbf{(21)}$$

As a result of this property, the WVD is often thought as a signal's energy distribution in the joint time-frequency domain. The STFT spectrogram possesses neither of the properties (3) or (4). Compared to the STFT spectrogram, the WVD has much better time and frequency resolutions. Measurements are taken by testing with beat signal of radar and results are provided in *Chapter 4*.

The main problem of the WVD is the *cross-term interference* i.e., the WVD of the sum of two signals is not the sum of their WVD's. If $s = s_1 + s_2$, it can be shown that

$$WVD_S(t,\omega) = WVD_{s_1}(t,\omega) + WVD_{s_2}(t,\omega) + 2\operatorname{Re}\{WVD_{s_1 s_2}(t,\omega)\} \qquad \textbf{(22)}$$

where the last term is the cross-WVD of s_1 and s_2 given by

$$WVD_{s_1 s_2}(t,\omega) = \int s_1\left(t + \frac{t'}{2}\right) s_2^*\left(t - \frac{t'}{2}\right) \exp\{-j\omega t'\}dt' \qquad \textbf{(23)}$$

Because this term reflects the correlation of two signal components, it is named the cross-term. As a result, if a signal contains more than one component in the joint time-frequency plane, its WVD will contain cross-terms that occur halfway between each pair of auto terms. The magnitude of these oscillatory cross terms can be twice as large as the auto terms. It is the cross-term interference that prevents the WVD from being used for real applications, though it possesses many desirable properties for signal analysis.

27

In the ensuing sections, we will discuss two alternative methods, the Cohen's class and the Gabor spectrogram. While the Cohen's class can be thought of as 2D linear filtering of the WVD that comprises the Smoothed Pseudo-WVD and Choi-Williams distribution, the Gabor spectrogram is a truncated WVD.

3.3.2 Cohen's Class of distributions

The Cohen's class of time-frequency distributions consists of a general class of bilinear distributions apart from the WVD. In the subsequent sub-sections, the general form of Cohen's class is discussed followed by specific distributions for reducing the cross-term interference problem in the WVD. It is defined as

$$C(t,\omega) = \int_{-\infty}^{\infty} e^{-j\omega\tau} \int_{-\infty}^{\infty} \Phi(t-\mu,\tau)s(\mu+\frac{\tau}{2})s^*(\mu-\frac{\tau}{2})d\mu d\tau \qquad \textbf{(24)}$$

The Fourier transform of $\phi(t,\mu)$, denoted as $\Phi(t,\mu)$ is called the kernel function. It can be easily seen that if $\Phi(t,\mu) = 1$, then $\phi(t,\mu) = \delta(t)$ and (24) reduces to the WVD defined in (19). Therefore, the WVD is a member of the Cohen's class. Other types of kernel functions can be designed to reduce the cross-term interference problem of the WVD. The prominent members of Cohen's class include the STFT-based spectrogram, the Choi-Williams distribution [13], the cone-shaped distribution [14] and the adaptive kernel representation [15].

3.3.2.1 Smoothed Pseudo-WVD

The definition of WVD (19) requires the knowledge of the quantity

$$q_s(t,\tau) = s(t+\tau/2)s^*(t-\tau/2) \tag{25}$$

which is difficult to be determined. So, we replace $q_s(t,\tau)$ in (25) by a windowed version of it, leading to the new distribution

$$PWVD_s(t,\upsilon) = \int_{-\infty}^{\infty} h(\tau)s(t+\tau/2)s^*(t-\tau/2)e^{-j2\pi\upsilon\tau}\,d\tau \tag{26}$$

where *h(t)* is a regular window. This distribution is called the *pseudo Wigner-Ville distribution*. This windowing operation is equivalent to a frequency smoothing of the WVD since

$$PWVD_s(t,\upsilon) = \int_{-\infty}^{\infty} H(\upsilon-\xi)W_s(t,\xi)\,d\xi \tag{27}$$

where *H(v)* is the Fourier transform of *h(t)*. Thus, because of their oscillating nature, the interferences will be attenuated in the pseudo-WVD compared to the WVD. The drawback with this kind of smoothing function is that it is controlled only by the short-time window $h(t)$; so we add a degree of freedom by considering a separable smoothing function

$$\Pi(t,\upsilon) = g(t)H(-\upsilon) \tag{28}$$

The tradeoff between time and frequency spread that spectrogram suffers from, is removed by the SPWVD, which allows a progressive and independent control, in both time and frequency, of the smoothing applied to the WVD.

The obtained distribution is

$$SPWVD_x(t,\upsilon) = \int\limits_{-\infty}^{\infty} h(\tau) \int\limits_{-\infty}^{\infty} g(s-t)x(s+\tau/2)x^*(s-\tau/2)ds\, e^{-j2\pi\upsilon\tau}\, d\tau \qquad (29)$$

The SPWVD is defined by a separable smoothing kernel $\Psi_T(t,f) = g(t)H(f)$ where g and h are two even windows with $h(0) = G(0) = 1$.

3.3.2.2 Choi-Williams Distribution

Choi and Williams [13] developed the theory of interference distributions and the ideas that allow one to design kernels to accomplish reduced interference in time-frequency distributions. They introduced the exponential kernel defined by

$$\Phi(\vartheta,\tau) = \exp\{-\frac{(\pi\vartheta\tau)^2}{2\sigma^2}\} \qquad (30)$$

where σ is a parameter. It is a product kernel and $\Phi(0,\tau) = \Phi(\vartheta,0) = 1$, which shows that both marginals are satisfied. Furthermore, this shows that it also satisfies the instantaneous frequency and group delay properties. The exponential kernel will suppress the cross-terms created by the two functions that have both different time and frequency centers. The parameter σ controls the decay speed, and as σ decreases the interference is reduced. On the other hand, when $\sigma \to \infty$, we obtain the WVD. So, we have a tradeoff in selecting the parameter value σ. The corresponding distribution is given by,

$$CWD(t,\omega) = \sqrt{\frac{2}{\pi}} \int\int \frac{\sigma}{|\tau|} e^{-2\sigma^2(s-t)^2/\tau^2} x\left(u+\frac{\tau}{2}\right)x^*\left(u-\frac{\tau}{2}\right)\exp\{-j\omega\tau\}du\,d\tau \qquad (31)$$

30

The kernel function is essentially a low pass filter in the (υ, τ) plane. It preserves all cross-terms that are on the υ-axis and τ-axis. As a result, the CWD usually contains strong horizontal and vertical ripples in the time-frequency plane. The horizontal ripples are caused by the auto-terms that have the same frequency center; the vertical ripples correspond to the auto-terms that have the same time center. The CWD preserves the property of the WVD while reducing cross-term interference.

3.3.2.3 Gabor Spectrogram

The Gabor expansion can be used to separate a signal's components in time and frequency as introduced in the previous sections. We first expand the signal into

$$s(t) = \sum_{m=-\infty}^{\infty} \sum_{n=-\infty}^{\infty} C_{m,n} h_{m,n}(t) \tag{32}$$

and then take the WVD on both sides to obtain

$$WVD(t,\omega) = \sum_{m=-\infty}^{\infty} \sum_{n=-\infty}^{\infty} \sum_{m'=-\infty}^{\infty} \sum_{n'=\infty}^{\infty} C_{m,n} C_{m',n'}^{*} WVD_{h,h'}(t,\omega) \tag{33}$$

where $WVD_{h,h'}(t,\omega)$ denotes the WVD of two time- and frequency shifted Gaussian functions. It can be shown that the energy of $WVD_{h,h'}(t,\omega)$ is inversely proportional to the rate of oscillation. Based on the closeness of $h_{m,n}(t)$ and $h_{m',n'}(t)$ in the time and frequency domains, we rewrite (33) as

$$GS_{D}(t,\omega) = \sum_{\left|m-m'\right|\left|n-n'\right| \leq D} C_{m,n} C_{m',n'}^{*} WVD_{h,h'}(t,\omega) \tag{34}$$

31

which is known as the Gabor spectrogram(GS), because it is a Gabor expansion-based-spectrogram. The parameter D in (34) denotes the order of GS. When D = 0, the GS only contains those terms in which $m=m^{'}$ and $n=n^{'}$ i.e., we consider the correlation of two identical components. As the order D increases, increasingly more less-correlated components are included. When D goes to infinity, the GS converges to the WVD.

3.4 Time-Variant Filter

An important application of joint time-frequency (TF) representation is in the detection and estimation of noise-corrupted signals. In the joint time-frequency domain, the signal-to-noise ratio is substantially improved since signal energy is concentrated in a small region compared to random noise that is spread throughout the region. The time-variant filter can be formed based on both linear and bilinear time-frequency representations with the former having better reconstruction structures. Hence, the Gabor expansion-based time-variant filter assumes significance. The problems associated with designing this filter is that for a given modified time-frequency representation, there may be no physically existing signal that corresponds to it. To overcome this problem, we have two techniques that are discussed below:

3.4.1 Least Square Error (LSE) filter

The procedure of the LSE filter is first to take the Gabor transform $G\overset{\smile}{s}$, where $\overset{\smile}{s}$ denotes the noise-corrupted signal vector and G the Gabor coefficients vector. Then, we mask the desired signal portion from the background noise to obtain noiseless Gabor coefficients

32

$$\hat{c} = \Phi G \overset{\prec}{s} \qquad \qquad (35)$$

where Φ denotes a mask vector (diagonal matrix) whose diagonal elements are either one or zero. Taking the Gabor expansion to compute the noise-reduced time waveform we have

$$\hat{x} = H\Phi G \overset{\prec}{s} \qquad \qquad (36)$$

where H is a synthesis matrix vector. H and G do not satisfy the dual relation except for critical sampling. Hence, the modified Gabor coefficients do not correspond to physically existing time function i.e.

$$G \hat{x} \neq \hat{c} \qquad \qquad (37)$$

The common approach is the LSE method, which finds the signal in the time-domain that minimizes the distance between signal's TF transform and the desired ones, i.e.

$$\Delta = \min \left\| \hat{c} - G \hat{x} \right\|^2 \qquad \qquad (38)$$

The solution of (38) is given by the pseudoinverse of G, that is,

$$\Delta_{opt} = (G^T G)^{-1} G^T \hat{x} \qquad \qquad (39)$$

The problem with the LSE filter is the computation of pseudoinverse, which is complicated in case of large number of samples. A more efficient algorithm is the *iterative algorithm*, which is described below.

3.4.2 Iterative Time-Variant Filter

The iterative time-frequency synthesis algorithm [8] was developed in the discrete Gabor transform domain [7]. It is proved that under the condition the algorithm converges to a signal that has its Gabor transform located exactly in a desired domain specified by the user in the TF plane. In the discrete Gabor transform domain, an L dimensional signal is transformed into an MN dimensional signal C and MN is greater than L due to oversampling. Therefore, only small sets of MN dimensional signals in the TF plane have their corresponding time waveforms with length L. Thus,

$$C = G_{MN \times L} s \text{ and } s = H_{L \times MN} C \tag{40}$$

where G denotes the discrete Gabor transform (DGT) and H denotes the inverse- DGT. Let $D_{MN \times MN}$ denote the mask diagonal matrix. The iterative algorithm is given as follows:

$$
\begin{aligned}
s_0 &= s, \\
C_{n+1} &= D_{MN \times MN} G_{MN \times L} s_n \\
s_{n+1} &= H_{L \times MN} C_{n+1} \\
&\qquad\qquad {}_{n=0,1,2....}
\end{aligned}
\tag{41}
$$

The advantage with this kind of filtering is that, we need not compute inverse of matrices. Under the sufficient condition for iteration [16],

➢ The DGT of the limit $\hat{s}$ of iterative algorithm falls in the mask $D_{MN \times MN}$

➢ The result of the first iteration s_1 is equivalent to Δ computed by LSE method.

CHAPTER 4

4 Measurements & Results

4.1 Ideal Simulations

The time-frequency techniques are tested first with ideal cases such as sum of two frequency tones and chirp signals. Two cosine signals of different frequencies and amplitudes are generated at different instances of time.

$$x_1[n] = a\cos(2*\pi*f_1*n_1 Ts), a = 0.5; f_1 = 50KHz$$
$$x_2[n] = b\cos(2*\pi*f_2*n_2 Ts), b = 1; f_2 = 150KHz$$
$$x[n] = x_1[n] + x_2[n] \tag{42}$$

where $n_1 = 0 : 999, n_2 = 1250 : 2249$, $f_s = 1/Ts = 500Khz$

The sums of both the cosine signals are taken and the time-frequency transform viz. SPWVD is applied to it. Figure 6 illustrates the sum of two frequency tones wherein the top plot is time waveform with the first signal varying from 0-2 msec and the second signal from 2.5-4.5 msec, the left plot is the traditional power spectrum which shows two peaks at 50 KHz and 150 KHz. The middle plot is the desired time-dependant spectrum computed by the Smoothed pseudo Wigner-ville distribution (described in Section 3.3.2.1). The conventional power spectrum indicates that there are two different frequency tones, but it is not clear when these frequency tones occur. The time-dependant spectrum not only shows the two frequency tones at 50 KHz and 150 KHz, but also tells when they take place. The image frequencies are

shown at $(f_s/2 - f_1) \& (f_s/2 - f_2)$ i.e. 200 KHz and 100 KHz respectively. The differences in amplitudes are also indicated by the respective colormap scales of the frequency tones.
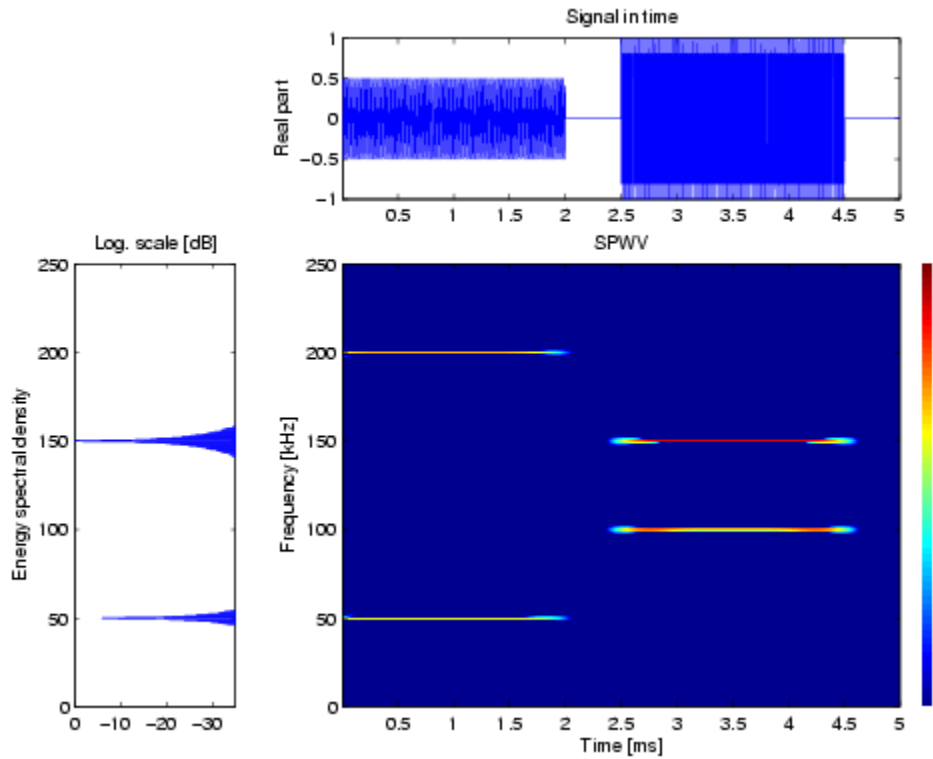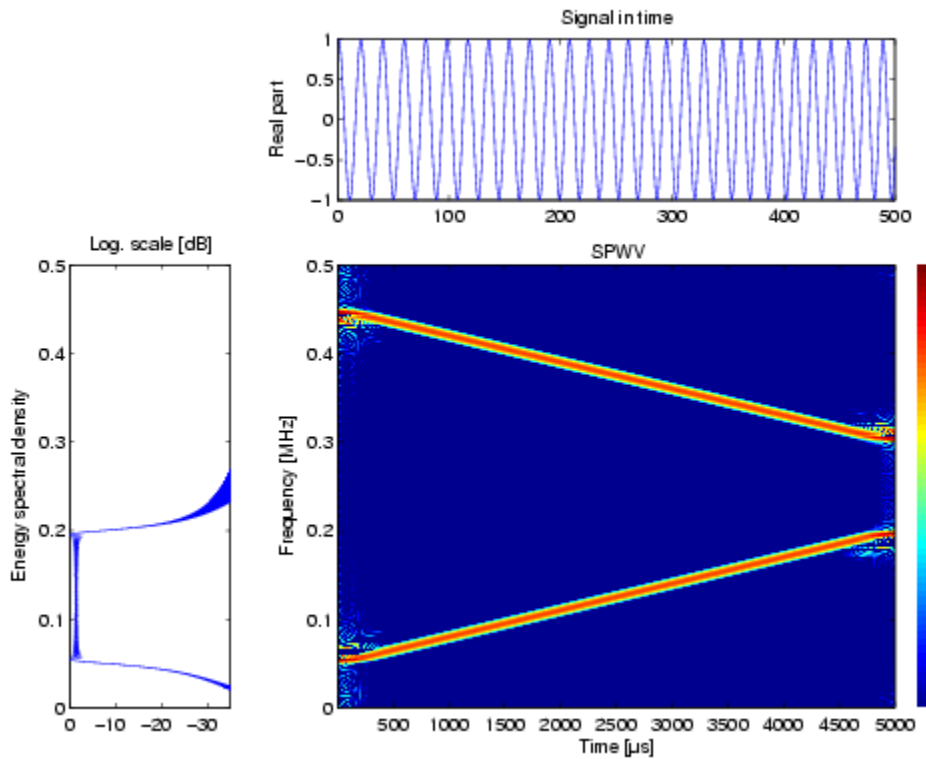

Figure 6: Time-frequency spectrum showing sum of two different frequency tones

Now, the time-frequency transform is tested against a linear chirp signal with a starting frequency of 50 KHz and bandwidth of 150 KHz. It is represented as follows:

$$s(t) = \cos(2\pi(f_0 t + \frac{1}{2}\alpha t^2)), \alpha = \frac{f_1 - f_0}{T}$$

(43)

where $f_0 = 50Khz, f_1 = 200Khz, T = 5m\sec$

Figure 7: Time-frequency spectrum showing linear chirp signal

Figure 7 shown above depicts the time-dependant spectrum viz. SPWVD applied to a linear swept-frequency signal. The time signal is maximized to show the chirp and the energy spectrum shows the positive spectrogram varying between 50 KHz and 200 KHz. The time-frequency spectrum is expressed in logarithmic scale with a threshold level of 1%. It shows a linear signal varying in time for the full duration of 5msec (*T*) as well as showing the frequency variation in the given bandwidth. The image frequency is shown as another chirp from 300-450 KHz.

The two cases discussed above suggested the validity of the time-frequency transform against ideal cases of a cosine and chirp signal. In the forthcoming sections, the radar beat signal will be tested against different time-frequency techniques and their advantages/disadvantages are discussed.

4.2 Sea-ice radar experimental data

The sea-ice (FMCW) radar described in *Chapter 2* was used to obtain experimental data set from field experiments which were conducted in Barrow, Alaska in May 2003. The measured sea-ice thickness will be compared with the depth from the radar calculated from signal processing experiments. The following graph shows some preliminary ice thickness transects from the EM-31 and drilling measurements taken from *Transect3*: 220m, sub-perpendicular to shore beginning opposite to BASC ~1 km from beach.
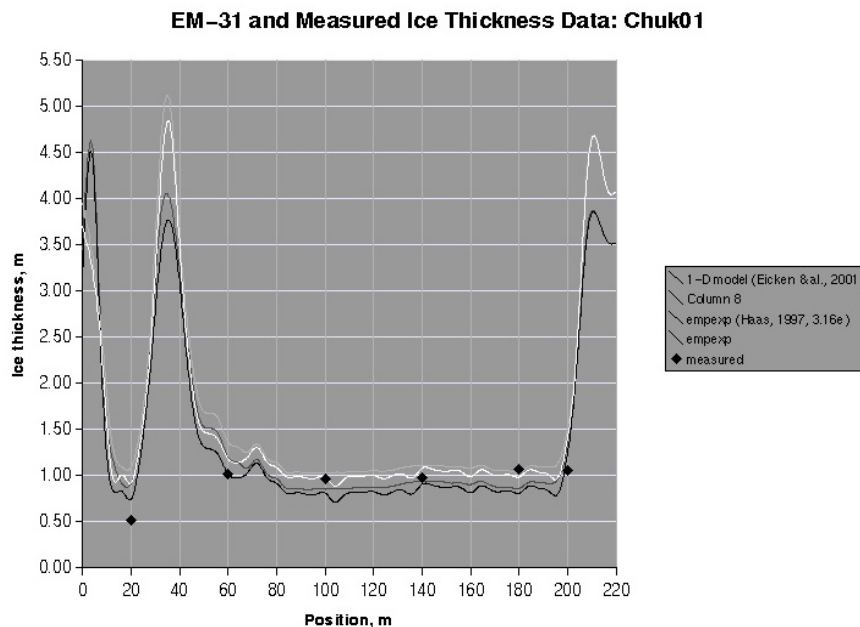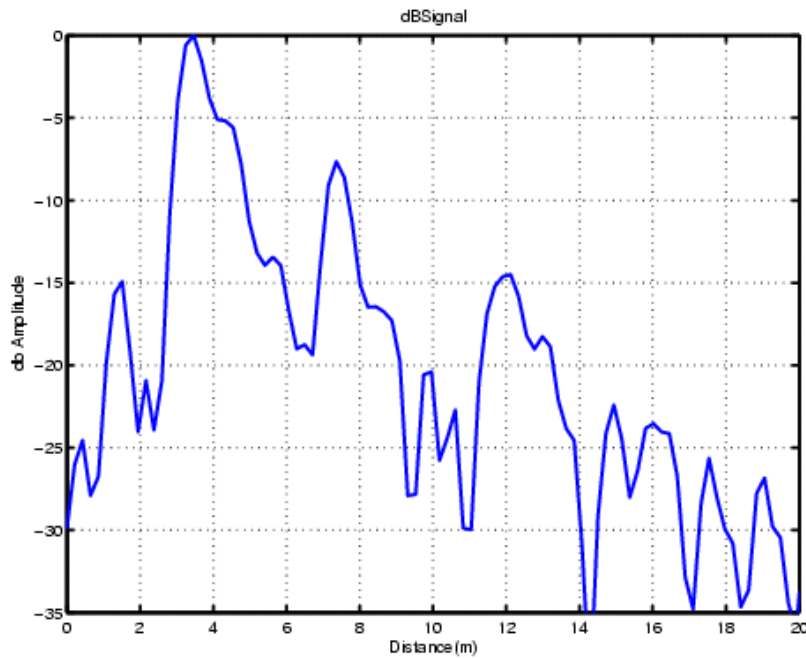

Figure 8: Transect 3 showing the measured sea-ice thickness depth

Here, the file *traverse2.bin* is used with particular reference to *Ascope-60* which is at a distance of 0-20 m from the first point as shown in the above graph. Figure 9 shows the Fourier spectrum of radar range profile:

Figure 9: Fourier spectrum of Ascope-60 in *traverse2.bin*

The antenna feed through is same as the *Top* of range profile since antenna is kept directly on top of ice. The antenna feedthrough is at a distance of 3.45m given by the maximum amplitude peak. The Fourier spectrum suggests that the ice-bottom is present at a distance of 7.35m that will be investigated further by the time-dependant spectrum to distinguish the layers clearly from the noise signals and multiples. These distance calculations are calculated from E*quation (2)* and it is assumed that speed of light is $c / \sqrt{3}$ where *c* is the free space velocity of light.

4.3 Time-frequency Distribution techniques

4.3.1 How does TFD distinguish the surface return from noise?

The time-dependant spectrum expresses the variation of the radar beat signal at different instances of time for a given frequency, the frequency expressed as a function of distance or range. If the signal is present for the entire duration of the time interval at a given frequency, a definite surface return (*Top* or *bottom*) is said to be present at the aforementioned location. If the signal is not present for the entire time-duration, it is assumed to be either a noise signal or a multiple layer. The time-frequency distribution does not distinguish between the noise & multiple returns. Any signal apart from the top or bottom return is considered to be noise.

4.3.2 Short-time Fourier transform

This technique is a linear transform which is a windowed version of the Fourier transform as described in *Section 3.2.1* which depicts the behavior of the signal as the block of window moves along the signal. Figure 10 shows the STFT spectrogram when a narrow window of 128 points is used. The spectrum below has a good time resolution with high resolution peaks well separated from each other in time viz. 2.2, 2.4 and 2.7msec. But, the drawback is that the frequency resolution is really bad with every peak covering a range of frequencies instead of a single frequency.
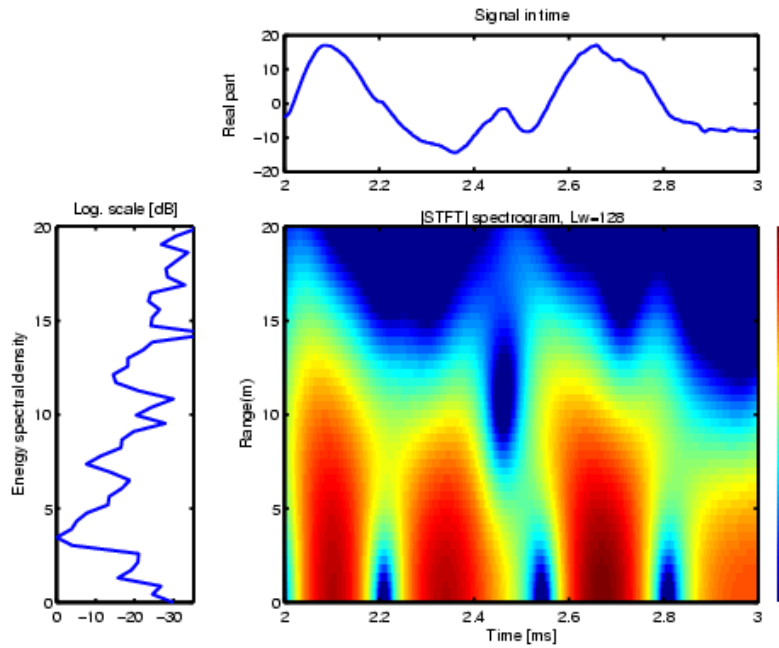
Figure 10: STFT spectrogram with narrow window

When we use a wide window, we get the results shown in Figure 11, it has a good frequency resolution with high resolution peaks at the respective positions comparing to the peaks in the energy spectrum, but the time-resolution has been completely lost compared to that shown in Figure 10. We cannot precisely determine the position of the layers because of loss in resolution in time-scale. Although the STFT-based spectrogram is simple and easily implemented, it has been found inadequate for the applications where both high time and frequency resolutions are required. Thus, we can summarize this technique as: if we choose a short window *h*, the smoothing window function will be narrow in time and wide in frequency, leading to a good time resolution but bad frequency resolution; and vice-versa.

41
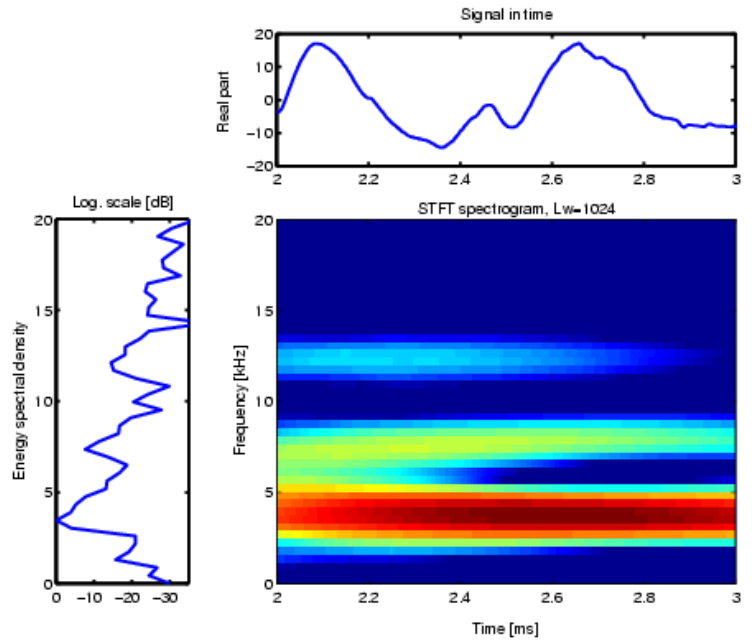
Figure 11: STFT spectrogram with wider window

This necessitates the need for a technique which has both good time & frequency resolution. The bilinear transforms which were described in Chapter 3 exhibit good resolutions. This helps to determine the layer returns at the exact locations. This will help to find out the measured depth from the radar and compare it with the measured results got from field experiments.

4.3.3 Wigner-Ville Distribution

This is a bilinear transform which characterizes a signal's properties better than the STFT-based spectrogram in the joint time-frequency domain as explained in *Section 3.3*.1. There is no window effect involved here.
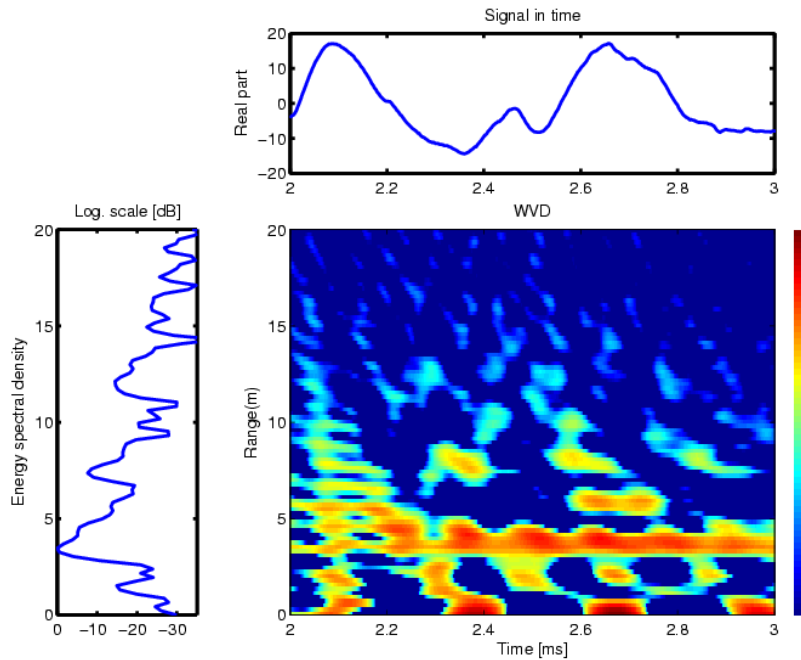
Figure 12: WVD of chirp signal showing surface return layers and interference terms

The top of the range profile is shown at a distance of around 3.5m in the power spectrum and we find a signal varying in all instances of time at that particular frequency in the Wigner-ville distribution with a very high colormap. Thus, we can conclude that this layer indeed is the antenna feed through. We also observe a signal around 7.5m that is present almost for the entire signal duration. This signal in the energy spectrum is around 6dB lower than the maximum amplitude peak which is also observed via the colormap time-dependant spectrum where yellow is around 6dB lower than the maximum color amplitude. The other layers are scattered around and in lower amplitudes of the colormap, thus they are classified as noise signals or multiples. However, there are cross-term interference components generated in-between the surface returns. The interference geometry suggests that two points of the time-frequency plane interfere to create a contribution on a third point which is located at

43

their geometrical midpoint. Besides, these interference terms oscillate perpendicularly to the line joining the two points interfering, with a frequency proportional to the distance between these two points. These cross-term interference effects can be removed by applying corresponding windows and smoothing distributions, which will be illustrated in the ensuing sections. In time-scale too, we observe respective peaks at the exact time instances shown in the plot above indicating that the WVD exhibits the best time-frequency resolution.
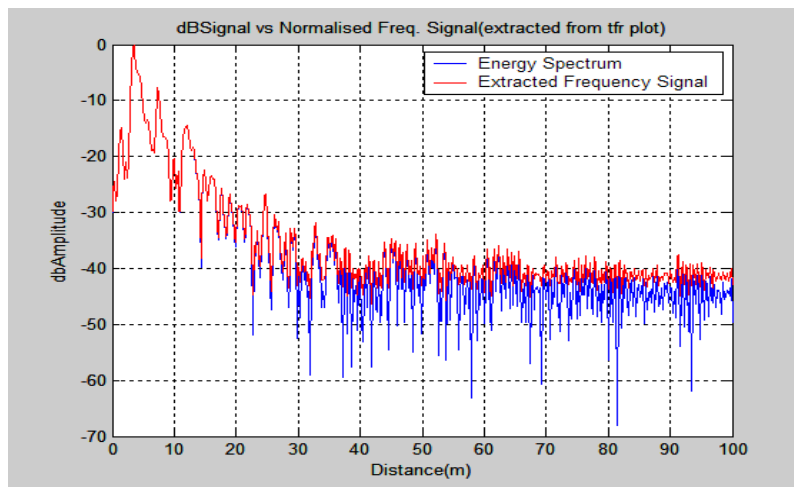
Figure 13 : WVD satisfying the marginal conditions

Figure 13 shows the WVD satisfying the marginal conditions. The blue plot shows the energy spectral density of a particular Ascope of range profile. The red plot shows the sum of TFR along the time axis, we see that we get back the power spectrum of the signal at a particular frequency. This proves that the WVD offers the best performance with the energy distribution optimally concentrated in the joint time-frequency domain.

4.3.4 Smoothed Pseudo WVD
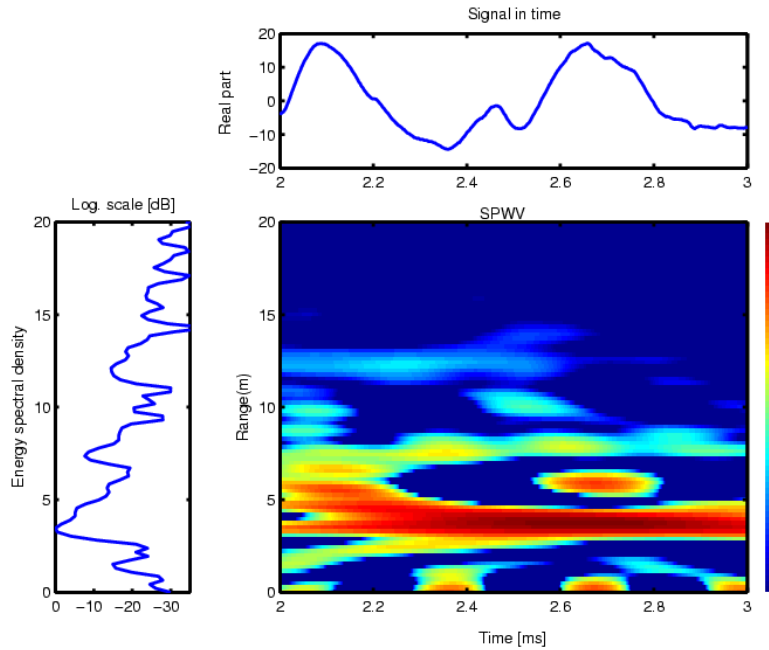
Figure 14: SPWVD of chirp signal with larger frequency window

The SPWVD overcomes the highly oscillatory cross-term effects of the Wigner-ville distribution by applying a low-pass filter; *g* and *H* which determine time and frequency smoothing independently. There is a compromise between the joint time-frequency resolution and the level of interference terms: the more we smooth in time and/or frequency, the poorer the resolution in time and/or frequency. In Figure 14, we have used a larger frequency smoothing window compared to the time smoothing window leading to a loss in frequency resolution compared to WVD in Figure 12. But, there is a considerable

improvement in the suppression of interference terms. The surface return layers are clearly visible, confirming the presence of these layers.

4.3.5 Choi-Williams Distribution

This technique is one of the prominent members of Cohen's class of time-frequency distributions which employs the use of weighting functions (or smoothing kernel functions) to reduce the cross-term interference as explained in *Section 3.3.2.2*
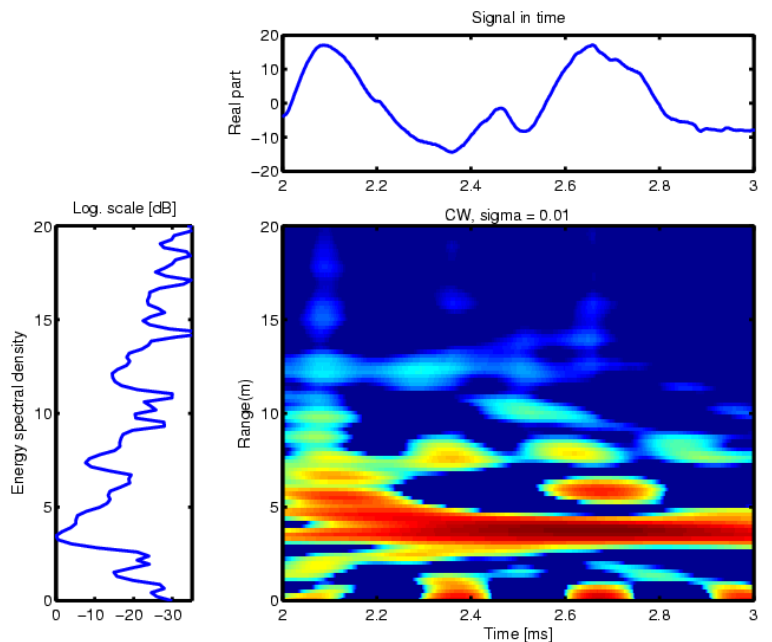
Figure 15: CWD of chirp signal with sigma=0.01

We will consider different cases where the size of kernel is varied. Let us consider initially the case where $\sigma = 0.01$ as in Figure 14. Here, the cross-terms diminish in size, width of the auto-term (i.e. signal) component spreads which enables the surface return layers to be distinguished easily; but there is a loss in resolution.
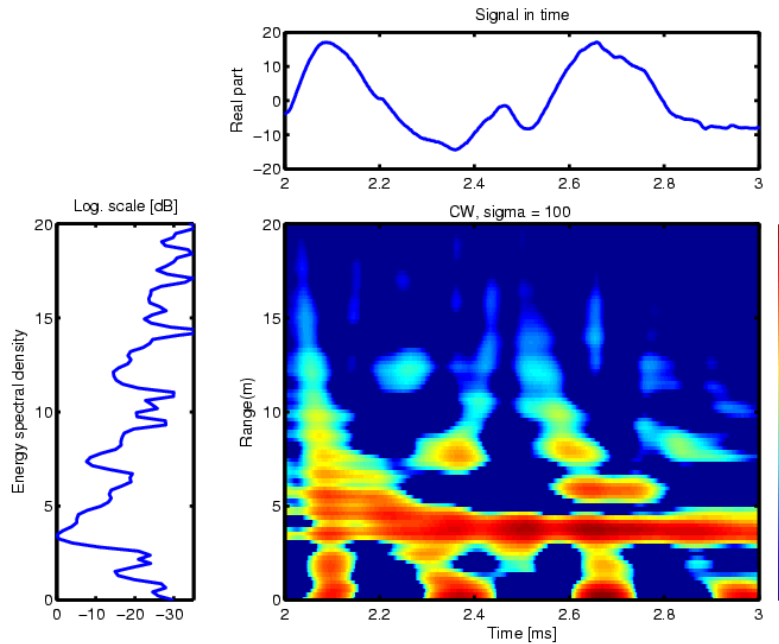
Figure 16: CWD of chirp signal with sigma=100

Now, when the scaling factor is increased and it approaches ∞, the CWD approaches the Wigner transform as the kernel becomes almost constant. This can be seen from Figure 16 where the interference terms between the layers becomes more prominent, distribution approaches the WVD as in Figure 12. The frequency & time resolution also become comparable to that of WVD.

4.3.6 Time-variant Filtering

The joint time-frequency distribution can be used for time-variant filtering of noisy signals as explained in *Section 3.4*. The Discrete Gabor transform is used for filtering in the time-frequency domain. Here, the radar beat signal is investigated for noise removal and to strengthen the signals of surface return. But, the problem encountered here is that the Gabor

47

transform which is used for filtering works well for moving target radars and does not possess enough frequency resolution to distinguish the surface returns clearly. Hence, this technique of time-variant filtering will *not* be suitable for sea-ice radar signal.

A suitable alternative to this time-variant filtering for removal of noise is the use of *'wavelet transform'*. This technique is currently being used for noise removal in '*depth sounder radar'* in RSL and is being found very effective. So, this can also be investigated for FMCW radars in the future. Figure 17 shows the radar echogram of the noisy signal which plots the number of A-scopes against the distance.
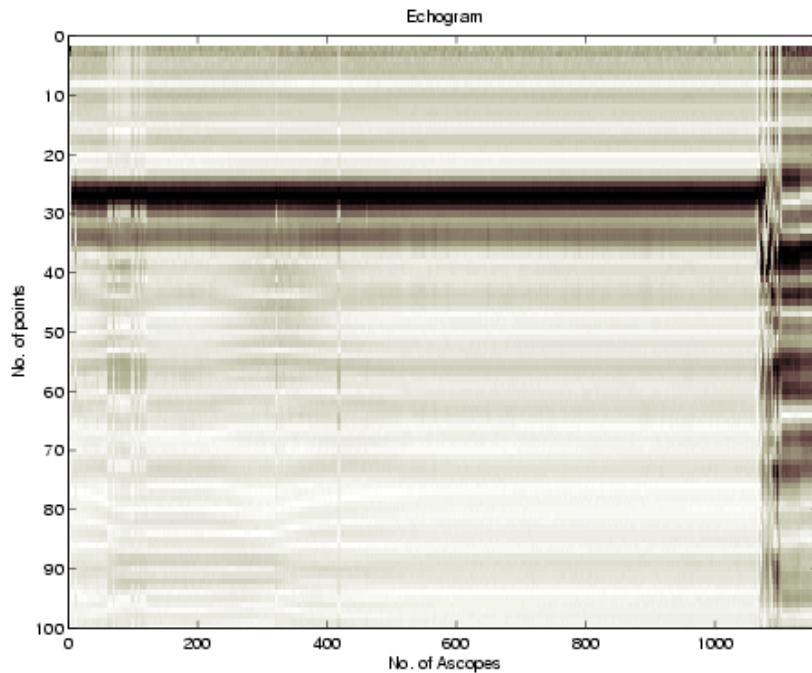
Figure 17: Echogram of noisy signal

The effects of noise removal for sea-ice radar include the echogram of denoised signal which is shown in Figure 18. Since the signal is quite clean, there is not much improvement in the SNR of denoised signal (there is only an increase of 1.4dB). But, this can definitely be investigated further to achieve better results by considering the appropriate mother wavelet for the particular radar and performing related signal processing. These will be discussed in detail in the recommendations for future work.
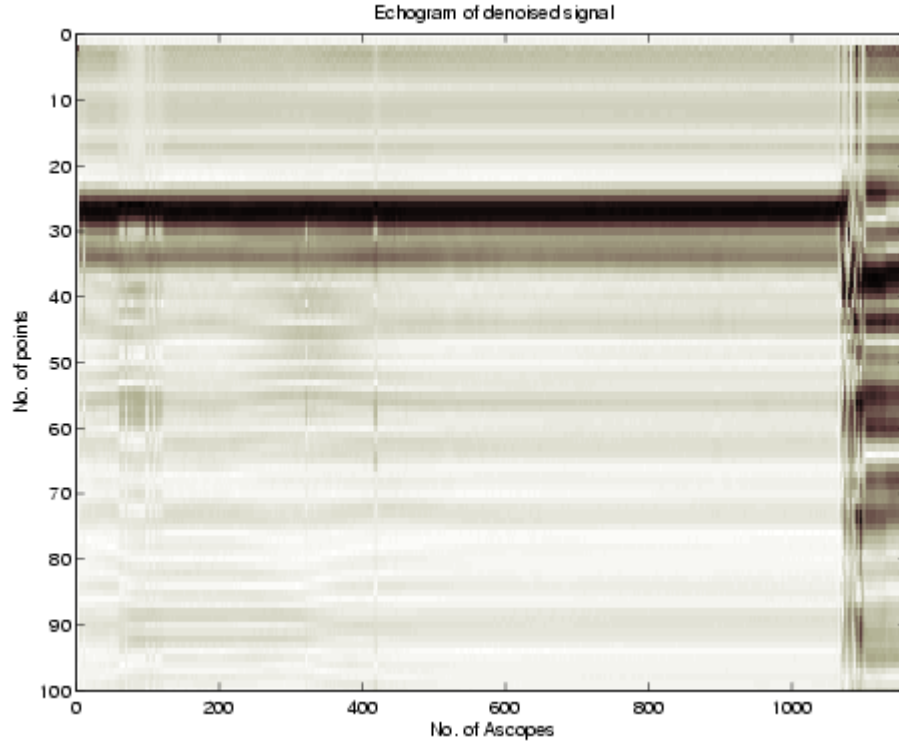
Figure 18: Echogram of denoised signal

CHAPTER 5

5   CONCLUSION & RECOMMENDATIONS

This project involved in providing an overview of the concepts and methods of joint time-frequency analysis and their application in FMCW radars. The major tools of time-frequency analysis are the inner product and expansion, similar to the Fourier transform. The highlights of the project include the following:

- Comparison between Fourier analysis and joint time-frequency analysis was provided and it was found that time-dependant spectra is a powerful tool for understanding the nature of those signals whose power spectra changes with time with particular reference to radar signals.

- The effect of time-frequency analysis was investigated for FMCW radars for determining the range profile and to distinguish the surface return layers from noise and multiple returns. Here, a brief description about the sea-ice radar designed in RSL, University of Kansas is mentioned and simulation results were validated against measured field test results.

- The joint time-frequency algorithms fall into two categories: linear and quadratic. While the STFT and Gabor expansion maps a signal between the time domain and the time-frequency domain, the bilinear transforms are more powerful and useful for real-time applications.

- The WVD gives the best resolution (in time and in frequency), but presents the most important interferences, whereas the STFT spectrogram gives the worst resolutions, but with nearly no interferences; the smoothed-pseudo WVD allows choosing the best compromise between these two extremes. The CWD is one of Cohen's class of distribution which is based on the smoothing kernel and approaches the WVD as scaling parameter increases.

- The different time-frequency distributions are first tested against ideal simulations of cosine and chirp signals. Then, the experimental radar beat signal is used for testing the different techniques. The *Top* and *ice-bottom* surface layers were clearly visible at the measured frequency for all instances of time confirming to the presence of a definite layer at that distance. The results from simulations i.e. depth from radar closely matched that of measured depth.

- Time – variant filtering procedures were investigated using discrete Gabor transform and it was not found suitable for these radar signals as it lacked a good frequency resolution to distinguish the surface returns clearly and was more suitable for moving targets.

Here are some useful recommendations for future work:

- Wavelet analysis is being used prominently for other types of radars such as *'depth sounder'* and its use can be investigated for future use with FMCW radars.

- Time –variant filtering can be attempted for other radar signals and particularly for those with moving targets

- The applications of JTFA can also be analyzed in detail for speech & music signal processing

REFERENCES

[1] Shie Qian and Dapang Chen, *Joint Time-Frequency Analysis: Methods and Applications*, NJ: Prentice Hall, 1996.

[2] Victor C. Chen and Hao Ling, *Time-Frequency Transforms for Radar Imaging and Analysis*, MA: Artech House Inc., 2002.

[3] D. Gabor, "Theory of Communications", *J.IEE*, vol. 93, no. III, pp. 429-457, November 1946

[4] T. Sparr, *"Time-frequency analysis for radar signal processing"*, FFIE, Norway

[5] S. Qian and Dapang Chen, "Discrete Gabor transform"*, IEEE Trans. Signal Processing*, vol. 41, no. 7, pp. 2429-2439, July 1993.

[6] V. Ramasami, S. Gogineni, B. Holt, P. Kanagaratnam, K. Gurumoorthy, S. K. Namburi, J.Henslee, D. Braaten, A. Mahoney and V.Lytle, "A low frequency wideband depth sounder for sea ice"*, submitted to IEEE International Geo-Science and Remote Sensing Society*, 21-25 July 2003. Toulouse, France.

[7] X.G. Xia and S. Qian, "An iterative algorithm for time-varying filtering in the discrete Gabor transform domain"*, IEEE Trans. Signal Processing*.

[8] X.G. Xia, "System identification using chirp signals and time-varying filters in the joint time-frequency domain"*, IEEE Trans. Signal Processing* vol. 45, no. 8, pp. 2072-2084, August 1997.

[9] F.Auger, P. Flandrin, P. Goncalves, O. Lemoine, *Time-frequency Toolbox: For use with Matlab,* 1996

[10] I. Daubechies, "The wavelet transform, time-frequency localization, and signal analysis", *IEEE Trans. Inform. Theory*, pp. 961-1005, September 1990.

[11] P. Kanagaratnam, *"Airborne Radar for High Resolution Mapping of Internal Layers in Glacial Ice to Estimate Accumulation Rate"*, Ph.D. Thesis, Electrical Engineering and Computer Science, The University of Kansas, 2002.

[12] K. Gurumoorthy, "*Design and Development of a Compact Low- Power Radar Data Acquisition System*", M.S. Thesis, Electrical Engineering and Computer Science, The University of Kansas, 2003.

[13] H. Choi and W.J. Williams, "Improved time-frequency representation of multicomponent signals using exponential kernels", *IEEE Trans. Acoust., Speech, Signal Processing* vol. 37, no. 6, pp. 862-871, June 1989.

[14] Y. Zhao, L.E. Atlas and R.J. Marks, "The use of cone-shaped kernels for generalized time-frequency representations of nonstationary signals", *IEEE Trans. Acoust., Speech, Signal Processing* vol. 38, no. 7, pp. 1084-1091, July 1990.

[15] R.G. Baraniuk and D.L. Jones, "A signal dependant time-frequency representation", *IEEE Trans. Signal Processing* vol. 41, no. 1, pp. 1589-1602, January 1994.

[16] X.G. Xia and S. Qian, "Convergence of an iterative time-variant based on discrete Gabor transform domain", *IEEE Trans. Signal Processing*.